FLOW RAPIDS

FLOW CAMBRIDGE
UNIVERSITY PRESS

Leveraging three-dimensionality for navigation in bluff-body wakes

Vedasri Godavarthi[1] (iD), Kartik Krishna[2], Steven L. Brunton[2] (iD) and Kunihiko Taira[1] (iD)

[1]Department of Mechanical and Aerospace Engineering, University of California Los Angeles, Los Angeles, CA, USA
[2]Department of Mechanical Engineering, University of Washington, Seattle, WA, USA
Corresponding author: Vedasri Godavarthi; Email: vedasrig@g.ucla.edu

Abstract

Biological flyers and swimmers navigate in unsteady wake flows using limited sensory abilities and actuation energies. Understanding how vortical structures can be leveraged for energy-efficient navigation in unsteady flows is beneficial in developing autonomous navigation for small-scale aerial and marine vehicles. Such vehicles are typically operated with constrained onboard actuation and sensing capabilities, making energy-efficient trajectory planning critically important. This study finds that trajectory planners can leverage three-dimensionality appearing in a complex unsteady wake for efficient navigation using limited flowfield information. This is revealed with comprehensive investigations by finite-horizon model-predictive control for trajectory planning of a swimmer behind a cylinder wake at Reynolds number of 300. The navigation performance of three-dimensional cases is compared with scenarios in a two-dimensional (2-D) wake. The underactuated swimmer is able to reach the target by leveraging the background flow when the prediction horizon exceeds one-tenth of the wake-shedding period, demonstrating that navigation is feasible with limited information about the flowfield. Further, we identify that the swimmer can leverage the secondary transverse vortical structures to reach the target faster than is achievable navigating in a 2-D wake.

Impact Statement

Recent advances in the development of small-scale autonomous vehicles require energy-efficient path planning strategies to enable navigation in highly unsteady flows. In this work, we investigate navigation in unsteady fluid flows, specifically how three-dimensional flow structures can be leveraged for effective navigation with limited temporal information of the flowfield. We study energy-efficient trajectory planning in 3D wake flows. This work shows that 3D vortical structures can be leveraged for energy-efficient navigation, and that their trajectories differ from the case of 2D wake flows.We identify successful navigation strategies using limited temporal prediction capabilities, and hence have the potential to develop sensor-based autonomous vehicle navigation strategies in complex 3D unsteady flows.

1. Introduction

Small-scale aerial and marine vehicles are gaining traction in applications typically considered high risk for manned vehicles. For these operations, vehicles need to traverse unsteady flows, such as flying in urban environments (Watkins *et al.*, 2020), in the wake of artificial and natural structures and navigating behind large marine vehicles for maritime operations (Shukla & Sinha 2015). Such wake flows are associated with strong unsteady three-dimensional (3-D) vortical disturbances. Autonomous vehicles

often experience adverse effects when encountering such flows without prior information (Zereik *et al.*, 2018).

There have been studies on the effect of wake flows on the stability and performance of biological flyers and swimmers. The effect of 3-D vortical perturbations generated by unsteady bluff-body wakes on the aerodynamic coefficients and moments of insect flight and hummingbird flight show variable responses depending on the orientation and relative strength of the vortical perturbations (Ortega-Jimenez *et al.*, 2014; Shyy *et al.*, 2016). The effect of three-dimensionality on locomotion is also studied in fish swimming (Lauder 2015; Liao 2007; Maia *et al.*, 2015) where fish undulate relative to the vortical structures for energy-efficient navigation. These studies have been conducted at high speeds and also consider the interaction between the swimmer/flyer with the flowfield. Understanding how the 3-D flow structures can be leveraged for navigation offers insights into biological locomotion and the development of autonomous navigation strategies. Hence, we consider trajectory planning for laminar 3-D wakes.

Over recent years, there has been extensive research on trajectory-planning strategies for the navigation of autonomous vehicles in complex background flows. Given complete knowledge of the underlying environment, optimisation methods such as graph-based algorithms (Kularatne *et al.*, 2016), and stochastic optimisation (Subramani & Lermusiax 2016) have been used to obtain optimal trajectories. Recently, reinforcement learning has been utilised for navigation in unsteady flows using limited local information (Colabrese *et al.*, 2017; Gunnarson *et al.*, 2021; Jiao *et al.*, 2021). Additionally, the Lagrangian coherent structure (LCS) theory has been used for energy-efficient path planning (Senatore & Ross 2008). Krishna *et al.*, 2022 proposed a finite-horizon model-predictive control approach to identify energy-efficient trajectories and their connection to LCSs for navigating unsteady flows.

In this study, we investigate the effect of three-dimensionality on navigation in unsteady wakes using the finite-horizon model-predictive control approach used in Krishna *et al.*, 2022. We consider underactuated point swimmers navigating in the 3-D wake of a cylinder at a Reynolds number of 300, where the flow exhibits three-dimensionality due to secondary instabilities, and compare their performance when navigating in 2-D wakes. We reveal that secondary vortices in 3-D flow facilitate faster navigation with limited information. The paper is outlined as follows. The computational set-up and the flow physics of the cylinder flow are introduced in section 2. The finite-horizon model-predictive control approach is discussed in section 3. Section 4 provides the results for trajectory planning in cylinder wakes. The conclusions are given in section 5.

2. Computational set-up

We consider a 3-D incompressible wake behind a circular cylinder obtained from a direct numerical simulation (DNS) at a diameter (D) based on a Reynolds number, $Re = U_\infty D/\nu$ of 300, where U_∞ and ν are free-stream velocity and kinematic viscosity, respectively. The simulation is performed using the incompressible flow solver Cliff, (Cascade Technologies Inc.) based on a second-order accurate finite volume method for spatial discretisation and a fractional-step method for time stepping (Ham & Iaccarino 2004; Ham *et al.*, 2006). The computational domain extends to $-20 \leq x/D \leq 30$ in the streamwise direction. The transverse extent is $-40 \leq y/D \leq 40$ and the spanwise extent is $0 \leq z/D \leq 4$ to capture the wavenumber of secondary instabilities with a uniform discretisation of 80 grid cells and a time step of $\Delta t = 0.005$. Hybrid grids are used with a structured mesh close to the cylinder and an unstructured mesh in the far-field region. We also obtain a 2-D flow over a cylinder at the same Reynolds number using the same domain in the x, y directions. It amounts to approximately 0.1 and 8.3 million cells for 2-D and 3-D wakes, respectively. Further details on the computational set-up can be found in Kim *et al.*, 2024. For finite-horizon trajectory planning and visualisation, we choose a subdomain $(x/D, y/D, z/D) \in [-2, 10] \times [-2, 2] \times [0, 2]$.

3. Finite-horizon model-predictive control

We use a finite-horizon model-predictive control (MPC) approach developed by Krishna *et al.*, 2022 to perform trajectory optimisation of a point swimmer. The swimmer dynamics is modelled as

$$\dot{\boldsymbol{x}}(t) = \boldsymbol{v}(\boldsymbol{x}(t), t) + \boldsymbol{u}(t), \tag{3.1}$$

where $\boldsymbol{x}, \boldsymbol{u} \in \mathbb{R}^n$ are the position vector and actuation velocity of the swimmer while $\boldsymbol{v}$ is the background flow velocity and $n = 2, 3$ for 2-D and 3-D flows. The background flow velocity is obtained from the DNS of the cylinder wake. When the actuation velocity is zero, the swimmer acts as a passive drifter. The swimmer dynamics is numerically integrated using a time step of $\Delta t = 0.05$. The actuation velocity is determined from the MPC optimisation of the cost function given by

$$J = \int_{t_0}^{t_0 + T_H} [\boldsymbol{e}(\tau)^T \mathbf{Q} \boldsymbol{e}(\tau) + \boldsymbol{u}(\tau)^T \mathbf{R} \boldsymbol{u}(\tau)] d\tau, \tag{3.2}$$

subject to constraints on the component-wise actuation velocity with $|u_i(t)| \leq \eta_i$, where η_i is the actuation velocity bounds on the ith velocity component. Here, T_H is the time horizon over which the cost function is minimised, and $\boldsymbol{e}$ is the error of the current state from a target state, $\boldsymbol{x}(t)$, $\boldsymbol{e}(t) = \boldsymbol{x}(t) - \boldsymbol{x}_{\text{target}}$. The matrix $\mathbf{Q} \in \mathbb{R}^{n \times n}$ is positive semi-definite and penalises the state error throughout the trajectory, and $\mathbf{R} \in \mathbb{R}^{n \times n}$ is a positive definite matrix penalising the actuation effort. Here, the actuation velocity of the swimmer is penalised, although the acceleration could also be optimised.

For the current problem, $\mathbf{Q}$ is set to the identity matrix. When the actuation velocity is large i.e. $|u| \geq U_\infty$ (free stream), the trajectory reaches the target directly. We consider underactuated scenarios to see how the swimmer exploits the background flow. The local background velocity for the cylinder wake varies in the streamwise, transverse and spanwise (x, y, z) directions, with the streamwise velocity being dominant. Thus, the actuation efforts are penalised differently in different directions, and $\mathbf{R}$ is a diagonal matrix where the ith diagonal element is given as $R_{ii} = \gamma_i$ and γ_i is the actuation penalisation in the ith direction. The time horizon T_H is another key parameter, as larger T_H requires larger predictive capabilities i.e. more temporal information about the background flow to the swimmer.

4. Navigating three-dimensional wake flows

We consider trajectory planning for wake crossing in 2-D and 3-D cylinder wakes at $Re = 300$ as a canonical problem to examine the effect of three-dimensionality on swimmer navigation. At this Re, the secondary instabilities (referred to as modes A and B) result in three-dimensionality (Williamson 1996). Modes A and B are developed in the vortex cores (seen as less coherent spanwise vortices due to vortex tilting (Aleksyuk & Heil 2023)) and the braid regions between consecutive spanwise vortices (seen as streamwise-elongated vortices in figure 1(a)), respectively. These secondary instabilities result in the aperiodic nature of wake flow with a dominant frequency of $St = 0.202$, contrary to the periodic flow at a frequency $St = 0.212$ developed over a 2-D cylinder at the same Re.

We consider wake-crossing scenarios (around 60 samples). These trajectories are shown in red in figure 1(a). The start (filled circles) and target transverse y locations are on either side of the cylinder wake ($y < 0$ for start and $y > 0$ for target positions) on the same spanwise plane. The streamwise x locations are chosen randomly in the cylinder wake. The background flow is initialised at the same phase of vortex shedding for both 2-D and 3-D flows. We consider five different initial phases of vortex shedding as the starting background flow for all the samples. Since the optimisation function is performed for each component, the penalisation for actuation velocity is also performed component-wise. For these wake-crossing scenarios, the swimmer is sensitive to actuation in a transverse direction, i.e. when not penalised in the transverse direction, the swimmer reaches the target in a straight line, as discussed later. Here, we present the underactuated cases with actuation bounds on the velocity as $0.9, 0.2, 0.5$ in the x, y, z directions with R_{ii} using $(\gamma_1, \gamma_2, \gamma_3) = (0.1, 10, 0.1)$. The time horizon for all cases is chosen
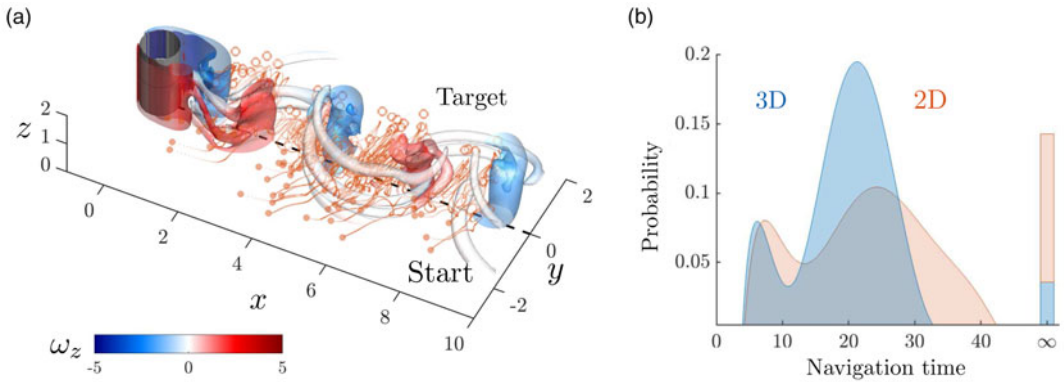
Figure 1. *Trajectories of swimmers crossing the wake for 3-D flow over a cylinder at Re = 300 visualised using an iso-surface of Q-criterion Q = 0.5, coloured by spanwise vorticity ω_z in (a) isometric view. (b) Probability distribution of total navigation time in 2-D and 3-D wakes.*
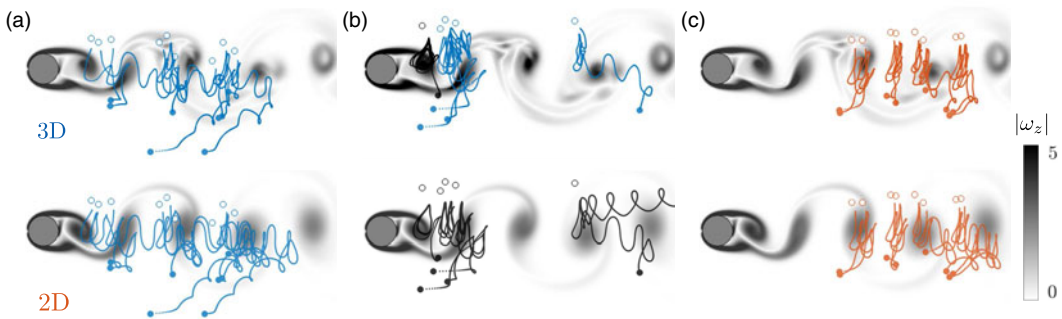

Figure 2. *An xy-view of wake-crossing trajectories in 3-D (top row) and 2-D (bottom row) wakes visualised using $|\omega_z|$ for when (a) 3-D navigation is faster (blue), (b) navigation in 2-D cannot reach the target (black) and (c) navigation times in 2-D and 3-D wakes are similar (red).*

as $T_H = 10\Delta t \approx 0.1 T_p$, where T_p is the dominant wake-shedding period. The time horizon can also be measured relative to the size of the vortical structures in the flowfield. The wavelength of the mode B (Λ_B) instability, resulting in the braid-like region, is $\Lambda_B = 0.8D$ (Barkley & Henderson 1996), hence this time horizon translates to 0.5 convective time units based on the diameter of the cylinder and 0.625 time units relative to the size of the braid-like structures. This indicates that flowfield information of approximately one half of the size of these vertical structures is enough for successful navigation. The obtained trajectories for $T_H \geq 0.1 T_p$ indicate that the swimmers can reach the target when the time horizon is approximately at least one-tenth of a period. For $T_H = 10$, the same trends are observed for $0.85 \leq \eta_1 \leq 0.95, 0.1 \leq \eta_2 \leq 0.3, 0.1 \leq \eta_2 \leq 0.5$. An instance of the effect of spanwise actuation bounds on the swimmer trajectory is discussed in the Appendix (depicted in figure 4). Since the optimisation strategy minimises $\|e(t)\|$ in (3.2), we consider the swimmer to be successful when $\|e(t)\| \leq \epsilon D$, which in this study is set to $\epsilon = 1/3$.

To compare the navigation performance in 2-D and 3-D wakes, we use the navigation time N_T, the time taken by the swimmer to reach the target, as a performance metric. The probability distribution of N_T for the sampled scenarios averaged over the three different initial background flow conditions is visualised in figure 1(b). We observe that distribution is shifted toward lower N_T for 3-D wake navigation identifying faster navigation in 3-D wakes. The probability distribution also shows cases when $N_T \to \infty$ for unreachable scenarios, Thus the swimmers navigating in a 3-D wake are more likely to reach the target position while being faster than those navigating in a 2-D wake.
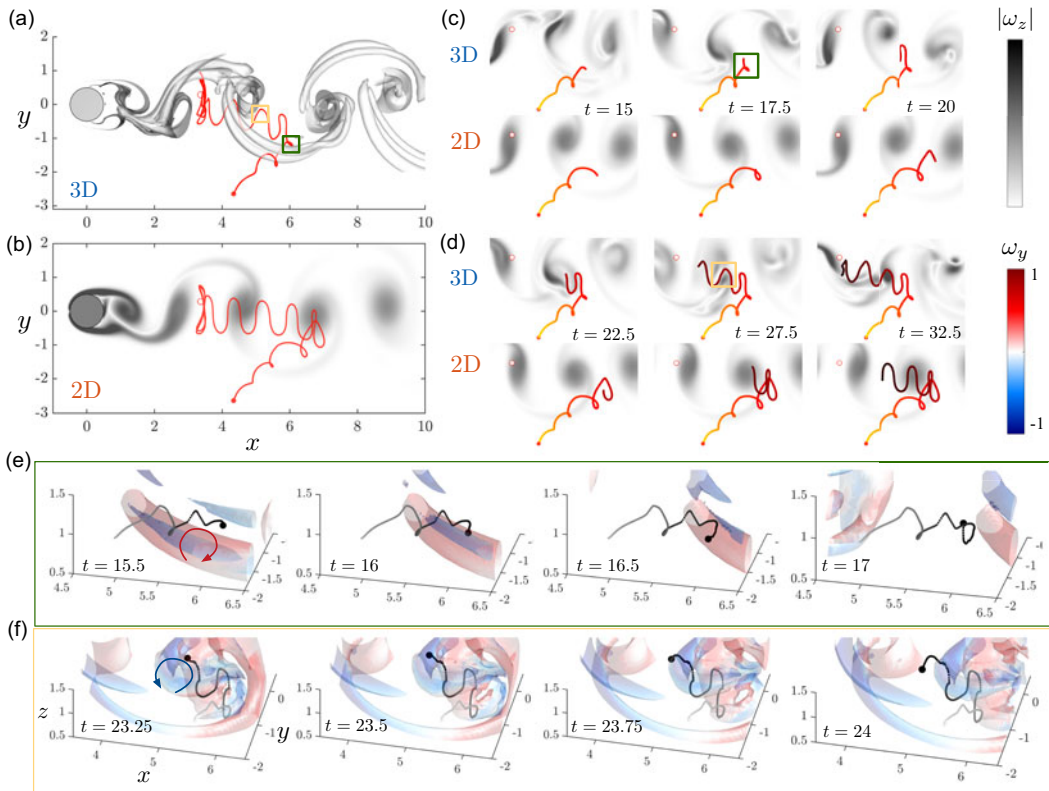
Figure 3. *Trajectory optimisation for a wake-crossing scenario in (a) 3-D and (b) 2-D wakes visualised using $|\omega_z|$. (c–d) Instantaneous trajectories during the navigation in 3-D (top) and 2-D (bottom) wakes. (e–f) Zoomed-in view of the evolution swimmer trajectory and background flow visualised using $Q = 0.1$ and coloured using ω_y in a 3-D wake.*

We divide the obtained trajectories into three scenarios as depicted in figure 2: (i) when the 3-D navigation is faster than the 2-D one (blue in figure 2a), (ii) when swimmers cannot reach the target (black in figure 2b) and (iii) when navigation in two dimensions is faster than in a 3-D wake (red in figure 2c). For (iii), the navigation time difference is approximately 20% of the wake-shedding period ($-\Delta N_T < 0.2T_p$). The main difference between (i) and (iii) is the initial traverse locations y_0 (filled circles): for (i) they are outside of the wake whereas for (iii) the start locations are in the wake region, resulting in lower background velocity from the start. From figure 2(a), the underactuated swimmer traverses significantly in the streamwise direction before reaching the target, whereas in figure 2(c) we observe that, due to the current actuation parameters and the initial and target locations of the swimmer relative to the cylinder wake, the swimmer can directly cross the wake (almost in a straight line). This shows that streamwise navigation is faster in 3-D wakes.

Figure 2(b) shows such cases where the swimmer fails to reach the target location in a 2-D wake (black) but succeeds in a 3-D wake (blue). The transverse target locations $y_{target} > 1.4D$ (unfilled circles) are farther from the wake, located in the free stream, for these cases. The 2-D navigation with a finite horizon fails whereas the 3-D wake navigation succeeds. Although the target locations are in the free stream, the secondary vortices in the braid regions in a 3-D wake provide low-velocity regions, allowing the target to be reached and expanding the reachability boundaries. Even in a 3-D wake, there are locations too far from the wake where the swimmer fails to reach the target for a given time horizon (shown by the leftmost trajectory in black in figure 2b (top)).

We now investigate the flow physics that the swimmer leverages for faster navigation in 3-D wakes. We consider a scenario where 3-D wake navigation is faster ($\Delta N_T > 0$), as depicted in figure 3(a-b) with an initial location of $x_0 = (4.34, -2.65, 1.0)$ (denoted by filled circle) and the target position of $x_{\text{target}} = (3.36, 0.29, 1.0)$ (denoted by unfilled circle) and $\Delta N_T = 8.3 \approx 1.8 T_p$. In both 2-D and 3-D wake navigation, the swimmer initially travels downstream due to the lower actuation velocity of the swimmer compared with the background flow. A few time instants for the downstream navigation are shown in figure 3(c). We observe that the swimmer in a 3-D wake 'redirects' towards the goal earlier than that in a 2-D wake, as seen at $t = 17.5$, even though both the swimmers reach similar y locations. The swimmer in a 2-D wake travels farther downstream before it can redirect towards the target. Once the y location of the swimmer is in the cylinder wake, utilising the low background velocity the swimmer redirects and travels upstream in the wake towards the target, as shown in figure 3(d). The swimmer trajectory oscillates in the x and y directions relative to the spanwise vortices in the cylinder wake, with fewer oscillations observed in a 3-D wake compared with a 2-D wake. The upstream navigation trajectory in the 2-D wake in figure 3(b) is similar to the ones identified by Gunnarson et al. (2021), where the swimmer leverages the induced velocities in the x and y directions by the spanwise vortices.

The zoomed-in view of the time instants when the swimmer in a 3-D wake redirects towards the target (green box in figure 3a) and the time instants of the swimmer navigating upstream (yellow box in figure 3b) are shown in figure 3(e–f). The instantaneous swimmer location (black dot) and its trajectory (grey) are shown relative to a transverse vortex (shown using ω_y) as it induces velocity in x and z directions. Figure 3(e) depicts the swimmer navigation under the influence of a counter-clockwise vortex. From, $t = 15.5$ to $t = 17$, the swimmer first travels in the negative z direction ($t = 16, 16.5$) and then travels in the upstream (negative x) direction, ($t = 17$) following the induced velocity and the background flow, thereby redirecting toward the upstream target earlier than its 2-D counterpart.

For efficient upstream navigation in the 3-D wakes, two mechanisms are in play: (i) the vorticity in the transverse and streamwise directions and (ii) the reduced coherence of spanwise vortices. Figure 3(f) depicts the swimmer navigation under the influence of a clockwise transverse vortex while travelling upstream in the wake. From $t = 23.25$ to $t = 24$, the swimmer first travels in the positive z direction and then in the negative x direction ($t = 23.5, 23.75$), leveraging the local orientation of background flow caused by the transverse vortex. This shows that the swimmer in a 3-D wake travels in positive or negative z direction to effectively leverage the transverse vortices for upstream travel. The swimmer travels in the spanwise direction according to the orientation of subdominant transverse and streamwise vortices. These secondary vortices provide low-velocity regions and change the background flow orientation due to the induced velocity. The swimmer leverages these vortices through the spanwise motion to effectively 'redirect' toward the target for faster upstream navigation.

5. Conclusions

We investigated the influence of three-dimensionality on the navigation of underactuated swimmers in unsteady wakes using finite-horizon MPC for trajectory optimisation. We compared the obtained trajectories for navigation in 2-D and 3-D cylinder wakes at $Re = 300$. For both scenarios, the time horizon needed to reach the target is only one-tenth of the wake-shedding period. This makes trajectory optimisation for bluff-body wake navigation sensor friendly. We also identified that the swimmer can navigate faster in 3-D wakes compared with 2-D wakes for most scenarios. Through spanwise motion, the swimmer can effectively leverage the secondary vortices, specifically transverse vortices to redirect towards the target faster. The low coherence of spanwise vortices and the presence of secondary vortices also facilitate faster upstream navigation when compared with 2-D wake navigation.

Appendix

The underactuated swimmer trajectories shown in the main manuscript are obtained using the actuation bounds of $(\eta_1,\eta_2,\eta_3) = (0.9,0.2,0.5)$ in the x, y and z directions respectively. While the lower actuation bound in the y direction is needed to avoid crossing the wake in a straight line, we here address the effect of actuation bounds in the spanwise direction. Let us consider the scenario discussed in figure 3. Figure 4 shows the trajectory evolution of the swimmer when $\eta_3 = 0.2$ (red) and $\eta_3 = 0.5$ (blue). Here, we use the same actuation bounds of $(\eta_1,\eta_2) = (0.9,0.2)$ in x and y directions. We observe that both trajectories are similar irrespective of the difference in the actuation bound in the z direction. Since the secondary vortices are weaker than the spanwise vortices, the induced velocity by the secondary vortices in the z direction is also quite small, resulting in less actuation requirement in the z direction.
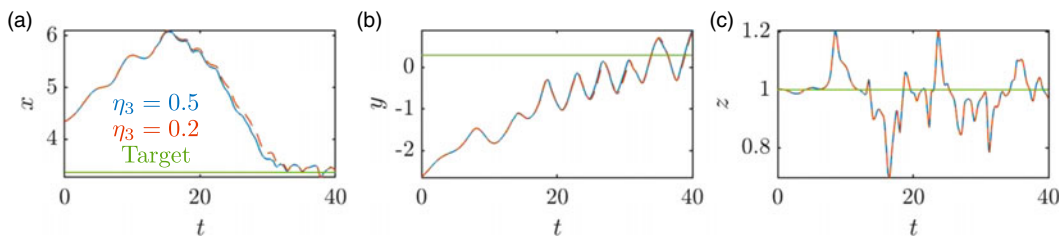

Figure 4. *Trajectory evolution for a wake-crossing scenario in a 3-D wake in the three directions for different actuation bounds in z-direction (η_3).*

References

Aleksyuk, A. I., & Heil, M. (2023). On the onset of long-wavelength three-dimensional instability in the cylinder wake. *Journal of Fluid Mechanics*, *967*, A23.

Barkley, D., & Henderson, R. D. (1996). Three-dimensional Floquet stability analysis of the wake of a circular cylinder. *Journal of Fluid Mechanics*, *322*, 215–241.

Colabrese, S., Gustavsson, K., Celani, A., & Biferale, L. (2017). Flow navigation by smart microswimmers via reinforcement learning. *Physical Review Letters*, *118*(15), 158004.

Gunnarson, P., Mandralis, I., Novati, G., Koumoutsakos, P., & Dabiri, J. O. (2021). Learning efficient navigation in vortical flow fields. *Nature Communications*, *12*(1), 7143.

Ham, F., & Iaccarino, G. (2004). *Energy conservation in collocated discretization schemes on unstructured meshes* . Annual Research Briefs, Center for Turbulence Research. (pp. 3–14).

Ham, F., Mattson, K., & Iaccarino, G. (2006). *Accurate and stable finite volume operators for unstructured flow solvers*. Annual Research Briefs, Center for Turbulence Research. (pp. 243–261).

Jiao, Y., Ling, F., Heydari, S., Heess, N., Merel, J., & Kanso, E. (2021). Learning to swim in potential flow. *Physical Review Fluids*, *6*(5), 050505.

Kim, Y., Godavarthi, V., Rolandi, V., Klamo, J., & Taira, K. (2024). Influence of three-dimensionality on wake synchronization of oscillatory cylinder. *Journal of Fluid Mechanics*, *1001*, A24.

Krishna, K., Song, Z., & Brunton, S. L. (2022). Finite-horizon, energy-efficient trajectories in unsteady flows. *Proceedings of the Royal Society A*, *478*(2258), 20210255.

Kularatne, D., Bhattacharya, S., & Hsieh, M. A. (2016). Time and energy optimal path planning in general flows. In *Proceedings of Robotics: Science and Systems*, 1–10.

Lauder, G. V. (2015). Fish locomotion: Recent advances and new directions. *Annual Review of Marine Science*, 7(1), 521–545.

Liao, J. C. (2007). A review of fish swimming mechanics and behaviour in altered flows. *Philosophical Transactions of the Royal Society B: Biological Sciences*, *362*(1487), 1973–1993.

Maia, A., Sheltzer, A. P., & Tytell, E. D. (2015). Streamwise vortices destabilize swimming bluegill sunfish (Lepomis macrochirus). *Journal of Experimental Biology*, *218*(5), 786–792.

Ortega-Jimenez, V. M., Sapir, N., Wolf, M., Variano, E. A., & Dudley, R. (2014). Into turbulent air: Size-dependent effects of von Kármán vortex streets on hummingbird flight kinematics and energetics. *Proceedings of the Royal Society B*, *281*(1783), 20140180.

Senatore, C., & Ross, S. D. (2008). Fuel-efficient navigation in complex flows. In *2008 American Control Conference, IEEE*. 1244-1248.

Shukla, S., Sinha, S. S., & Singh, S. N. (2019). Ship-helo coupled airwake aerodynamics: a comprehensive review. *Progress in Aerospace Sciences*, *106*, 71–107.

Shyy, W., Kang, C. K., Chirarattananon, P., Ravi, S., & Liu, H. (2016). Aerodynamics, sensing and control of insect-scale flapping-wing flight. *Proceedings of the Royal Society A*, *472*(2186), 20150712.

Subramani, D. N., & Lermusiaux, P. F. (2016). Energy-optimal path planning by stochastic dynamically orthogonal level-set optimization. *Ocean Modelling*, *100*, 57–77.

Watkins, S., Burry, J., Mohamed, A., Marino, M., Prudden, S., Fisher, A., Kloet, N., Jakobi, T., & Clothier, R. (2020). Ten questions concerning the use of drones in urban environments. *Building and Environment*, *167*, 106458.

Williamson, C. H. K. (1996). Three-dimensional wake transition. *Journal of Fluid Mechanics*, *328*, 345–407.

Zereik, E., Bibuli, M., Mišković, N., Ridao, P., & Pascoal, A. (2018). Challenges and future trends in marine robotics. *Annual Reviews in Control*, *46*, 350–368.